

Direct proof of unique magnetic and superconducting phases in superoxygenated high- T_c cuprates

L. Udby,¹ J. Larsen,² N. B. Christensen,² M. Boehm,³ Ch. Niedermayer,⁴ H. E. Mohottala,⁵
T. B. S. Jensen,² R. Toft-Petersen,^{2,6} F. C. Chou,⁷ N. H. Andersen,² K. Lefmann,¹ and B. O. Wells⁸

¹*Nanoscience Center, Niels Bohr Institute, University of Copenhagen, DK-2100 Copenhagen, Denmark*

²*Department of Physics, Technical University of Denmark, DK-2800 Kgs. Lyngby, Denmark*

³*Institut Laue-Langevin, 38042 Grenoble Cedex 9, France*

⁴*Laboratory for Neutron Scattering, Paul Scherrer Institut, CH-5232 Villigen PSI, Switzerland*

⁵*University of Hartford, West Hartford, Connecticut 06117, USA*

⁶*Helmholtz Zentrum Berlin für Materialien und Energie, D-14109 Berlin, Germany*

⁷*Center for Condensed Matter Sciences, National Taiwan University, Taipei 10617, Taiwan*

⁸*Department of Physics, University of Connecticut, Storrs, Connecticut 06269-3046, USA*

We present a combined magnetic neutron scattering and muon spin rotation study of the nature of the magnetic and superconducting phases in electronically phase separated $\text{La}_{2-x}\text{Sr}_x\text{CuO}_{4+y}$, $x = 0.04, 0.065, 0.09$. For all samples, we find long-range modulated magnetic order below $T_N \simeq T_c = 39$ K. In sharp contrast with oxygen-stoichiometric $\text{La}_{2-x}\text{Sr}_x\text{CuO}_4$, we find that the magnetic propagation vector as well as the ordered magnetic moment is independent of Sr content and consistent with that of the 'striped' cuprates. Our study provides direct proof that superoxygenation in $\text{La}_{2-x}\text{Sr}_x\text{CuO}_{4+y}$ allows the spin stripe ordered phase to emerge and phase separate from superconducting regions with the hallmarks of optimally doped oxygen-stoichiometric $\text{La}_{2-x}\text{Sr}_x\text{CuO}_4$.

PACS numbers: 74.72.Gh, 74.25.Ha, 75.25.-j, 74.10.+v

The many active degrees of freedom in transition metal oxides lead to intrinsic complexity with different electronic states being nearly degenerate. As a consequence nanoscale phase separation can be observed in such different materials as the CMR manganites and high-temperature superconducting (HTSC) cuprates [1, 2]. A central challenging theme is how dopant disorder influences the details of the phase separation in otherwise electronically similar systems and e.g. pins fluctuating order [3]. We address this issue by investigating the electronic properties of a HTSC system with two essentially different mechanisms of charge-carrier doping i.e. mobile oxygen ions and immobile Sr ions.

Starting from the Mott insulating and antiferromagnetic parent compound La_2CuO_4 (LCO), replacement of La by Sr leads to superconductivity above $x = 0.055$ in $\text{La}_{2-x}\text{Sr}_x\text{CuO}_4$ (LSCO) with the highest superconducting transition temperature, $T_c = 38$ K at $x \simeq 0.15$ (optimal doping) [4]. On the other hand, intercalation of a sufficient amount of excess oxygen in Sr-free samples to produce $\text{La}_2\text{CuO}_{4+y}$ (LCO+O) leads to even higher $T_c \simeq 42$ K [5] and less flux-pinning [6]. The origin of the differences in superconducting properties lies in the nature of the doping-processes: When oxygen-stoichiometric LSCO is formed by cooling through the liquid-solid phase transition at temperatures far above room temperature, a homogeneous but quenched disordered distribution of Sr on La sites is produced. By contrast, intercalated oxygen remains mobile down to much lower temperatures [7] where it tends to organise in well-ordered superstructures that can be observed in diffraction experiments [8], and over which there is a

partial degree of control [9, 10]. Combining magnetisation and muon spin rotation, we have recently discovered that even in samples containing quenched disordered Sr, intercalated oxygen facilitates optimal superconducting properties ($T_c^{\text{onset}} \simeq 40$ K and weak pinning) [11, 12]. It does so by promoting phase separation between regions of the sample that are non-magnetic (and superconducting) and regions with magnetic order. The local magnetic fields around the muon stopping site are similar [11] to those of the so-called stripe ordered materials $(\text{La,Nd})_{15/8}\text{Sr}_{1/8}\text{CuO}_4$ (LNSCO) and $\text{La}_{15/8}\text{Ba}_{1/8}\text{CuO}_4$ (LBCO) [13]. From elastic neutron scattering (ENS) experiments on these materials it is known that the magnetic order is characterised by two incommensurate magnetic propagation vectors, corresponding to two domains of modulated antiferromagnetic order [14–16]. An ENS study on LSCO+O, $x = 0.09$ reveal similar peaks [17], but a systematic exposition of the nature and possible evolution of magnetic and superconducting states in LSCO+O has been lacking.

In this Letter we present a ENS study of the magnetic properties of LSCO+O single crystals covering a broad range of Sr content, and investigate the superconducting properties using high transverse field muon spin rotation (HTF- μ SR). Using neutrons as a bulk-sensitive probe of magnetism, we provide direct evidence for the identity of the magnetic phases of our LSCO+O samples in terms of propagation vector and ordered magnetic moment. Moreover, we show that these characteristics are the same as those of stripe-ordered LNSCO and LBCO. Further, we find that the superconducting penetration depth of all samples are identical within our experimen-

tal errors and of a magnitude similar to that of optimally doped oxygen-stoichiometric LSCO.

All samples studied are the same single crystals also used in [11] with $x = 0.04, 0.065, 0.09$. They were float-zone grown in an optical furnace and post-oxidised (superoxygenated) through wet-chemical methods [5, 8]. The intercalation process was stopped after a long period of oxidation, always after the sample showed a single transition of $T_c^{onset} \sim 40$ K as recorded by SQUID measurements. The ENS studies were performed at the cold triple-axis spectrometers RITA-II and IN14 at the Paul Scherrer Institute (PSI), Switzerland and the Institut Laue-Langevin, France, respectively. Both spectrometers employed elastic scattering mode with $E_i = E_f = 5$ meV and 40' horizontal collimation before and after the sample. Be-filters removed higher-order contamination scattering from the monochromators. All Miller indices in this work refer to the orthorhombic $Bmab$ notation in reciprocal lattice units [rlu] based on the low temperature lattice parameters [18]. The muon data were recorded at the General Purpose Surface-Muon Instrument at PSI using a high (0.3 T) transverse field after fast (>1 K/min) cooling, since the SC properties are known not to change with cooling rate for the investigated crystals.

To set the stage for LSCO+O, we start by summarising the magnetic properties of oxygen-stoichiometric LSCO: In the magnetic phase the modulation period and direction depends strongly on Sr content x and a quartet of peaks are detected by ENS with $\delta \propto x$ [19] away from the anti-ferromagnetic position corresponding to modulated anti-ferromagnetic (m-AFM) order in the CuO planes. For $0.024 \lesssim x \lesssim 0.055$ the spin structure is rotated i.e modulated diagonally with respect to the Cu-O bonds [20–22]. For $x > 0.055$ the modulation is parallel to the Cu-O bonds with incommensurability saturating at $\delta \simeq 1/8$ for $x \simeq 1/8$ [19]. Long-range magnetic order with correlation length $\xi > 100$ Å is only found for $x \simeq 1/8$. In striking contrast with these characteristics of LSCO, Figure 1 shows several key results of our study: In all the investigated superoxygenated LSCO+O samples through the Sr doping range $x = 0.04 - 0.09$ at $T \sim 2$ K, we have observed a quartet of peaks by ENS at the *same* positions. The peaks at $\mathbf{Q} = (1 + \delta_H, \delta_K, 0)$ are compared in the left panel of Figure 1. We find for all x that the peaks are located $\delta_H \sim \delta_K \sim \delta = 0.123 \pm 0.004$ away from the antiferromagnetic point. This corresponds to m-AFM with periodicity of 8.1(3) unit cells parallel the Cu-O bonds as is also found in oxygen-stoichiometric LSCO $x \simeq 1/8$. That the incommensurability δ and the modulation direction is always the same in LSCO+O regardless of Sr doping x is however opposed to what is observed in oxygen-stoichiometric LSCO. The peaks of LSCO+O are sharp and instrumentally resolved for $x < 0.09$ as seen in the left panel of Figure 1. For $x = 0.09$ there is however a $\sim 30\%$ broadening which we previously found to result from the finite size of the m-AFM domains in

the sample [17, 23]. These domains are, however, at least 300–400 Å for all x . This periodicity and long correlation lengths of the m-AFM signal are similar to those of the zero-field magnetic signal observed in LCO+O [24, 25], oxygen stoichiometric LSCO with $x \simeq 1/8$ and the parallel stripes found in LNSCO and LBCO [14–16]. The spin correlation lengths in our LSCO+O samples are however much larger than in oxygen stoichiometric LSCO samples with comparable Sr content [19]. The temperature dependence of the m-AFM peak intensity for LSCO+O is shown in the right panel of Figure 1. It follows the same power-law dependence for all $x = 0.04 - 0.09$ with transition temperature $T_N = 39(3)$ K [26] which is also in contrast to oxygen stoichiometric LSCO where the intensity does not follow the usual power-law dependence for the lowest dopings [27] and T_N is much smaller and varies in the same Sr doping range [28].

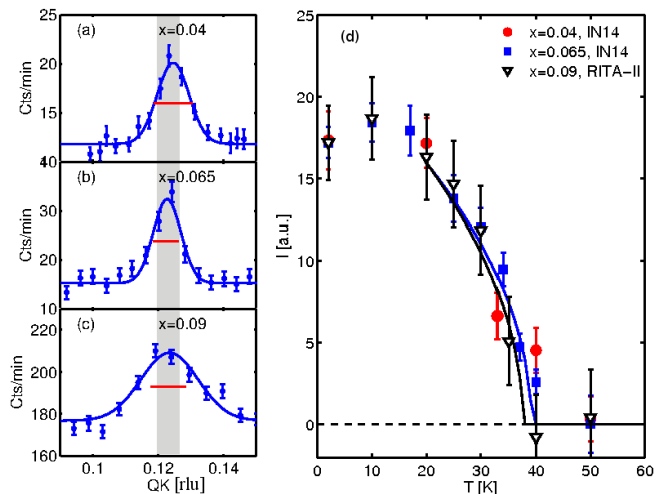


FIG. 1. (Color online) (a-c) ENS scans in reciprocal space through the m-AFM peak at $\mathbf{Q}=(1+\delta_H, \delta_K, 0)$. All data were taken at $T = 2$ K at IN14. Solid lines are Gaussian fits and the horizontal red lines show the resolution as found by corresponding scans through Bragg peaks. The grey shaded region indicates the average peak position as described in the text. (d) Temperature dependence of the intensity of the m-AFM peaks. The intensities are scaled at 2 K. In order to locate T_N , power-law fits with a fixed exponent $\eta = 0.5$ were conducted (lines).

In order to find the magnitude of the ordered magnetic moments from the ENS data we need knowledge of the magnetic volume fractions which can be provided by μ SR experiments. The muons stop at specific lattice positions and provide a random sampling of the internal field distribution both in the magnetic volume fraction and the vortex state of the superconducting volume fraction. All μ SR data presented in this Letter were fitted with a three-component model for the asymmetry following the procedure outlined in [29]. Two of the components are temperature dependent and related to the sample. A third component models the background orig-

inating from e.g. muons stopping in the cryostat walls or sample holder and is assumed to be temperature independent. For details see the supplementary information [18]. The first temperature dependent component models the muons which are rapidly relaxing, i.e. they are being depolarised by the ordered moments in the magnetic volume fraction of each sample for which the derived temperature dependence is shown in the top panels of Figure 2. We note that the magnetic volume fractions begin to grow at the same temperatures at which ENS reveals the onset of m-AFM order, see Figure 1(d), indicating that truly static magnetic order sets in below T_N . The second temperature dependent component is slowly relaxing and originates from the non-magnetic part of the sample. Its temperature dependence is also shown for each sample in the top panels of Figure 2. A slight decrease in precession frequency of this component [18] marks the superconducting onset transition at T_c . At base temperature we assume that all of this component originates from the flux-line lattice in the superconducting volume of the sample. The temperature dependence of the relaxation rate in the non-magnetic volume is shown in Figure 2. For all samples we observe a similar temperature dependence with $\sigma(T \rightarrow 0) \sim 0.9 \mu\text{s}^{-1}$. This value is the expected relaxation value for a superconducting volume with a penetration depth of at least $\lambda \sim 1500 \text{ \AA}$ [30] in an optimally doped LSCO sample with a rigid 3D vortex lattice. It is seen from these data that the relaxation rate increases below 40 K in all samples, coinciding with the superconducting transition temperature $T_c = 39(1) \text{ K}$. We have confirmed this by AC susceptibility measurements, regardless of the cooling rate. The magnetic and superconducting volume fractions and their transition temperatures are compiled in Table I. We note that the magnetic and superconducting transition temperatures coincide for all x .

x	V_m [%]	V_{SC} [%]	T_N [K]	T_c [K]
0.04	56(4)	44(1)	~ 40	39(1)
0.065	19(1)	81(1)	39(1)	38.7(7)
0.09	47(1)	53(1)	38(2)	37.1(5)

TABLE I. Collected μSR results for the magnetic and superconducting base temperature volume fractions, V_m and V_{SC} , respectively, of each sample. T_N and T_c are determined from ENS (Fig. 1) and μSR (Fig. 2 (d-f)), respectively.

We now return to the derivation of the magnetic moment from the ENS data based on the acquired knowledge of the magnetic volume fractions. Table II shows the integrated, mass-normalised peak areas of the m-AFM peaks from the ENS data, and it is seen that the intensity varies substantially, probably due to differences in both magnetic volume fraction and sample mosaic details. Hence, we normalise the m-AFM peaks to the integrated area of a Bragg peak and divide by the magnetic volume frac-

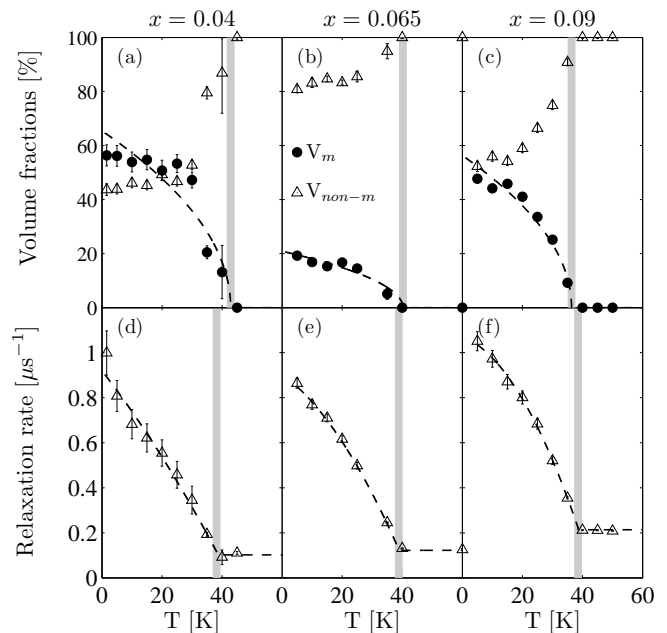


FIG. 2. Results of HTF- μSR experiments. If not visible, the statistical errors are smaller than the datapoint markers. (a-c) Temperature dependence of the magnetic and non-magnetic volume fractions of the sample. Dashed lines are guides to the eye and grey shaded regions mark T_N . (d-f) Temperature dependence of the spin relaxation rate for muons stopping in the superconducting regions of the sample. Following [31] the dashed lines are fits to the function $\sigma_0(1 - aT - bT^2)$ for $T < T_c$. Grey shaded regions mark T_c .

x	m [g]	I_{IC} [$\frac{\text{cts}}{\text{min}\cdot\text{g}}$]	I_{200} [$\frac{\text{cts}}{\text{min}\cdot\text{g}}$]	$A = \frac{I_{IC}}{I_{200}\cdot V_m}$
0.04	0.035	2.9(5)	$3.7(3)\cdot 10^4$	$1.4(3)\cdot 10^{-4}$
0.065	0.091	2.0(3)	$6.4(2)\cdot 10^4$	$1.6(3)\cdot 10^{-4}$
0.09	0.415	1.7(3)	$2.0(1)\cdot 10^4$	$1.8(3)\cdot 10^{-4}$

TABLE II. Mass (m), mass-normalized IC AFM and nuclear Bragg peak intensities, I_{IC} and I_{200} , respectively. The intensities derive from Gaussian fits to data taken under identical experimental conditions at IN14. The last column shows I_{IC} normalized by the product of I_{200} and the magnetic volume fraction V_m .

tion to obtain the constant A listed in Table II. It is seen that A is the same for all LSCO+O samples within errors, thus implying they have the same ordered magnetic moment if the same model for the magnetic order can be assumed. We thus turn to the specifics of the symmetry-related peaks in order to motivate a model for the spin-structure. For all LSCO+O samples we have observed peaks at the same positions $\mathbf{Q}_m = (1 \pm \delta_H, 0 \pm \delta_K, 0)$ and $(0 \pm \delta_H, 1 \pm \delta_K, 0)$ indicating a similar spin structure. For the $x = 0.09$ sample, full scans at all above mentioned positions were performed and the data fitted to Gaussian lineshapes as shown in Figure 3. The intensities and widths of all the m-AFM peaks are found to be the same

within two standard deviations as is also observed for the spin stripes in LNSCO [16] and LBCO [32]. We therefore assume, analogously to LNSCO, that the m-AFM peaks in LSCO+O in one direction can be represented by a simple collinear spin stripe model and the other set of peaks in the quartet are generated by 90° rotation between alternating CuO planes. For each CuO plane we consider a 8×2 Cu-site unit cell $[\uparrow\uparrow\downarrow \cdot \downarrow\uparrow\downarrow \cdot ; \downarrow\uparrow\downarrow \cdot \uparrow\uparrow\downarrow \cdot]$ where the moments are lying in the CuO plane with angle β with \mathbf{Q}_m . Then the magnetic structure factor is given by $|F_m|^2 = p^2 f_m^2 \mu^2 \sin^2 \beta |\tilde{F}_m|^2$. For $S=1/2$ spins we have $p = 0.2696 \cdot 10^{-14}$ m, and the form factor for Cu^{2+} and geometrical structure factor take the values $f_m = 0.90(5)$ [33] and $|\tilde{F}_m|^2 = 93.25$ at the m-AFM points. Details of this and the following calculations are shown in the supplementary material [18]. Based on the experimentally determined factor A in Table II we find the ordered moment in units of Bohr magnetons to be

$$\mu = \sqrt{|F_m|^2 / p^2 f_m^2 \sin^2 \beta |\tilde{F}_m|^2} = 0.10(2)\sqrt{C} / \sin \beta \quad (1)$$

Assuming that the spins are weakly correlated between neighboring CuO planes, the vertical resolution correction gives $C \simeq 1.4$ [18] and we obtain $\mu = 0.12(2)\mu_B$ for spins oriented along [010] ($\sin \beta = 0.99$) as in La_2CuO_4 [34] and $\mu = 0.17(3)\mu_B$ for spins oriented along [110] ($\sin \beta = 0.7(1)$), as observed in LNSCO [16]. If the scattering intensity is approximately constant along c^* (scattering rods) due to e.g. twinning as seen in LCO+O [24] we have $C \simeq 2.7$ and the quoted ordered moments must be corrected by a numerical factor ~ 1.4 . In the absence of experimental information about the c -axis magnetic correlations, we restrain ourselves to the conclusion that the ordered magnetic moments in the magnetic volume fractions of LSCO+O are of the same order of magnitude as the those determined for LCO+O ($\mu = 0.15(5)\mu_B$ [24]) and stripe ordered LNSCO ($\mu = 0.10(3)\mu_B$ [35]).

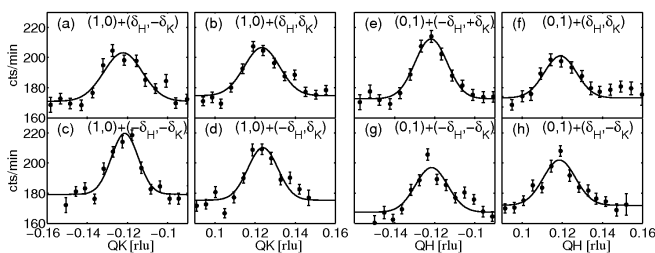


FIG. 3. (a-h) Rocking curve scans through the IC AFM peaks of LSCO+O $x = 0.09$. All lines represent Gaussian fits.

We summarise our results of LSCO+O through a range of Sr dopings to conclude that superoxygenation facilitates the same type of long-range m-AFM order, with same periodicity $\delta \sim 1/8$, moment and transition temperature $T_N = 39(3)$ K within errors. This is in contrast to oxygen stoichiometric LSCO [19, 21, 28]. Further-

more, the magnetic transition temperatures of the studied LSCO+O crystals are the same within errors whether determined using the local μSR probe or bulk-sensitive neutron scattering. This is also in contrast to oxygen stoichiometric LSCO where the transition temperature as observed by μSR is significantly lower than the one observed by neutron scattering due to gradual freezing of the moments [36]. These observations are evidence of the existence of a single and long-range ordered m-AFM phase throughout the Sr doping range $0.04 \leq x \leq 0.09$ in LSCO+O which is similar to the striped systems LBCO [14, 32] and LNSCO [15, 16, 37, 38]. Since our LSCO+O crystals stay orthorhombic at low temperatures, the stripe-like magnetic order is not pinned by the strong ordering field of the low temperature tetragonal (LTT) phase as in LBCO and LNSCO [14, 15]. However, the commensurate nature of the ordering still implies a strong coupling to the lattice. We expect that the difference here is that since LSCO+O has a weaker, random disordering field from the Sr dopants it also does not require the stronger lattice ordering field associated with the LTT phase. This picture is consistent with our observation that the LSCO+O sample with the highest Sr content $x = 0.09$ has slightly reduced magnetic correlation length.

Regarding the superconducting phase of LSCO+O, the transition temperature $T_c = 39(1)$ K is the same within errors and coinciding with the magnetic transition temperature for all samples in contrast to $T_c \propto x$ in oxygen-stoichiometric LSCO [19]. T_c is also not suppressed as in the anomalous 1/8 state of LNSCO [39] and LBCO [40] suggesting phase separation rather than competition between the two phases in the same areas of the sample. Furthermore the penetration depth is similar in the superoxygenated system throughout the investigated Sr range and has value corresponding to that of optimally doped LSCO. This is in contrast to oxygen stoichiometric LSCO where the penetration depths for superconducting samples increase with x [41]. The similarity of the temperature dependence of the relaxation rate in LSCO+O indicates that the superconducting gap symmetry is similar throughout the Sr doping range.

These observations prove that a long-range electronic phase separation occurs in LSCO+O between a 1/8 stripe-like magnetic phase and a superconducting phase which is similar to optimally doped LSCO. A recent report on pressure studies of LBCO [42] has μSR and magnetisation data similar to our earlier work [11] revealing phase separation between stripe-like magnetism and superconductivity. Despite these striking similarities between LSCO+O and pressurised LBCO, the latter seems to favor an underdoped, reduced T_c superconducting phase perhaps by depinning the charge order [43]. This differs from the superoxygenated samples we describe here where the separate phases appear to have different effective charge densities.

We thank Brian M. Andersen for helpful discussions. This work was supported by the Danish Agency for Science Technology and Innovation under the Framework Programme on Superconductivity and the Danish Research Council FNU through the instrument center DAN-SCATT. Work at the University of Connecticut was supported by the U.S. Department of Energy under Contract No. DE-FG02-00ER45801. This work is based on experiments performed partly at the Institut Laue-Langevin, Grenoble, France and partly at the Swiss spallation neutron source SINQ, Paul Scherrer Institute, Villigen, Switzerland.

-
- [1] E. Dagotto, *Science* **309**, 257 (2005).
- [2] G. Alvarez, M. Mayr, A. Moreo, and E. Dagotto, *Phys. Rev. B* **71**, 014514 (2005).
- [3] S. A. Kivelson, I. P. Bindloss, E. Fradkin, V. Oganesyan, J. M. Tranquada, A. Kapitulnik, and C. Howald, *Rev. Mod. Phys.* **75**, 1201 (2003).
- [4] H. Takagi, T. Ido, S. Ishibashi, M. Uota, S. Uchida, and Y. Tokura, *Phys. Rev. B* **40**, 2254 (1989).
- [5] A. Wattiaux, J.-C. Park, J.-C. Grenier, and M. Pouchard, *C. R. Acad. Sci. Paris* **310**, 1047 (1990).
- [6] F. Chou, D. Johnston, S.-W. Cheong, and P. Canfield, *Physica C* **216**, 66 (1993).
- [7] X. Xiong, P. Wochner, S. C. Moss, Y. Cao, K. Koga, and M. Fujita, *Phys. Rev. Lett.* **76**, 2997 (1996).
- [8] B. O. Wells, R. J. Birgeneau, F. C. Chou, Y. Endoh, D. C. Johnston, M. A. Kastner, Y. S. Lee, G. Shirane, and J. M. Tranquada, *Z. Phys. B* **100**, 535 (1996).
- [9] Y. S. Lee, F. C. Chou, A. Tewary, M. A. Kastner, S. H. Lee, and R. J. Birgeneau, *Phys. Rev. B* **69**, 020502 (2004).
- [10] M. Fratini, N. Poccia, A. Ricci, G. Campi, M. Burghammer, G. Aeppli, and A. Bianconi, *Nature* **466**, 841 (2010).
- [11] H. E. Mohottala, B. O. Wells, J. I. Budnick, W. A. Hines, C. Niedermayer, L. Udby, C. Bernhard, A. R. Moodenbaugh, and F. C. Chou, *Nature Mat.* **5**, 377 (2006).
- [12] H. E. Mohottala, B. O. Wells, J. I. Budnick, W. A. Hines, C. Niedermayer, and F. C. Chou, *Phys. Rev. B* **78**, 064504 (2008).
- [13] B. Nachumi *et al.*, *Phys. Rev. B* **58**, 8760 (1998).
- [14] M. Fujita, H. Goka, K. Yamada, J. M. Tranquada, and L. P. Regnault, *Phys. Rev. B* **70**, 104517 (2004).
- [15] J. M. Tranquada, B. J. Sternlieb, J. D. Axe, Y. Nakamura, and S. Uchida, *Nature* **375**, 561 (1995).
- [16] N. B. Christensen, H. M. Rønnow, J. Mesot, R. A. Ewings, N. Momono, M. Oda, M. Ido, M. Enderle, D. F. McMorrow, and A. T. Boothroyd, *Phys. Rev. Lett.* **98**, 197003 (2007).
- [17] L. Udby, N. H. Andersen, F. C. Chou, N. B. Christensen, S. B. Emery, K. Lefmann, J. W. Lynn, H. E. Mohottala, C. Niedermayer, and B. O. Wells, *Phys. Rev. B* **80**, 014505 (2009).
- [18] See Supplemental Material [URL by publisher].
- [19] K. Yamada *et al.*, *Phys. Rev. B* **57**, 6165 (1998).
- [20] M. Fujita, K. Yamada, H. Hiraka, P. M. Gehring, S. H. Lee, S. Wakimoto, and G. Shirane, *Phys. Rev. B* **65**, 064505 (2002).
- [21] S. Wakimoto *et al.*, *Phys. Rev. B* **61**, 3699 (2000).
- [22] M. Matsuda, M. Fujita, K. Yamada, R. J. Birgeneau, M. A. Kastner, H. Hiraka, Y. Endoh, S. Wakimoto, and G. Shirane, *Phys. Rev. B* **62**, 9148 (2000).
- [23] L. Udby, P. K. Willendrup, E. Knudsen, C. Niedermayer, U. Filges, N. B. Christensen, E. Farhi, B. O. Wells, and K. Lefmann, *Nucl. Instr. Meth. A* **634**, 138 (2011).
- [24] Y. S. Lee, R. J. Birgeneau, M. A. Kastner, Y. Endoh, S. Wakimoto, K. Yamada, R. W. Erwin, S. H. Lee, and G. Shirane, *Phys. Rev. B* **60**, 3643 (1999).
- [25] B. Khaykovich, Y. S. Lee, R. W. Erwin, S.-H. Lee, S. Wakimoto, K. J. Thomas, M. A. Kastner, and R. J. Birgeneau, *Phys. Rev. B* **66**, 014528 (2002).
- [26] We have too few points in the ENS data to fit a proper T_N for the small $x = 0.04$ crystal, but $T_N \sim 40\text{K}$ is consistent with the μSR data as discussed later in the text.
- [27] S. Wakimoto *et al.*, *Phys. Rev. B* **60**, R769 (1999).
- [28] K. Hirota, *Physica C* **357-360**, 61 (2001).
- [29] E. J. Ansaldo, J. H. Brewer, T. M. Riseman, J. E. Schirber, E. L. Venturini, B. Morosin, D. S. Ginley, and B. Sternlieb, *Phys. Rev. B* **40**, 2555 (1989).
- [30] Y. J. Uemura *et al.*, *Phys. Rev. B* **38**, 909 (1988).
- [31] J. E. Sonier *et al.*, *Phys. Rev. Lett.* **72**, 744 (1994).
- [32] M. Fujita, *Physica C* **481**, 23 (2012).
- [33] S. Shamoto, M. Sato, J. M. Tranquada, B. J. Sternlieb, and G. Shirane, *Phys. Rev. B* **48**, 13817 (1993).
- [34] D. Vaknin, S. K. Sinha, D. E. Moncton, D. C. Johnston, J. M. Newsam, C. R. Safinya, and H. E. King, *Phys. Rev. Lett.* **58**, 2802 (1987).
- [35] J. M. Tranquada, J. D. Axe, N. Ichikawa, Y. Nakamura, S. Uchida, and B. Nachumi, *Phys. Rev. B* **54**, 7489 (1996).
- [36] M.-H. Julien, *Physica. B* **329-333**, 693 (2003).
- [37] J. Chang *et al.*, *Phys. Rev. B* **78**, 104525 (2008).
- [38] J. Wen, Z. Xu, G. Xu, J. M. Tranquada, G. Gu, S. Chang, and H. J. Kang, *Phys. Rev. B* **78**, 212506 (2008).
- [39] M. K. Crawford, R. L. Harlow, E. M. McCarron, W. E. Farneth, J. D. Axe, H. Chou, and Q. Huang, *Phys. Rev. B* **44**, 7749 (1991).
- [40] A. R. Moodenbaugh, Y. Xu, M. Suenaga, T. J. Folkerts, and R. N. Shelton, *Phys. Rev. B* **38**, 4596 (1988).
- [41] Y. J. Uemura *et al.*, *Phys. Rev. Lett.* **62**, 2317 (1989).
- [42] Z. Guguchia, A. Maisuradze, G. Ghambashidze, R. Khasanov, A. Shengelaya, and H. Keller, *arXiv:1303.3865v1* (2013).
- [43] M. Hücker, M. v. Zimmermann, M. Debessai, J. S. Schilling, J. M. Tranquada, and G. D. Gu, *Phys. Rev. Lett.* **104**, 057004 (2010).